Digital Signal Processing 99 (2020) 102674

Contents lists available at ScienceDirect

Digital Signal Processing

www.elsevier.com/locate/dsp

Transmit beamformer design with a PAPR constraint to trade-off between beampattern shape and power efficiency

Ömer Çayır *, Çağatay Candan

Department of Electrical and Electronics Engineering, Middle East Technical University (METU), 06800, Ankara, Turkey

ARTICLE INFO

Article history:
Available online 23 January 2020

Keywords:
Transmit beamforming
Narrowband beamforming
Wideband beamforming
Peak-to-average power ratio
Alternating direction method of multipliers
Radar waveform design

ABSTRACT

This study examines the effect of peak-to-average power ratio (PAPR) constraint on the transmit beamformer design problem with the goal of establishing a trade-off between the power efficiency (maximizing the average transmitted power) and other metrics such as the power level fluctuation in mainlobe, peak-sidelobe level (PSL), etc. Typically, unimodular weights are utilized in transmit beamforming to maximize the average transmitted power. Yet, unimodular weights maximize the power efficiency at the expense of other performance metrics. It is shown that even a slight relaxation of the design problem from the unimodular condition (PAPR $= 1$), say setting PAPR $\leqslant 1.1$, results in a significant improvement in other performance metrics at a negligible loss of power efficiency. To achieve the trade-off between the metrics, an alternating direction method of multipliers (ADMM) based solution to the transmit beamformer design is given. The suggested solution is applicable to both narrowband and wideband beamformers and also to some other related problems such as the unimodular radar waveform design (code design) problem.

1. Introduction

In a conventional narrowband transmit beamformer, each antenna element transmits the same low-pass equivalent signal scaled by a chosen complex-valued weight. The problem of transmit beampattern design is to determine the weights such that several requirements such as flat-top beampattern, low sidelobes, power efficiency, etc. are satisfied. Typically, unimodular weights (weights with a constant magnitude) are used in transmit beamforming to maximize the transmission power. The power maximization is important to extend the instrumented range of the sensor, which is proportional to (average power $\times$ aperture)$^{1/4}$ [1], and also to improve the signal-to-noise ratio (SNR) affecting the accuracy of estimation operations conducted by the sensor. In addition to the transmit power maximization, a beampattern with a flat mainlobe and low sidelobes is highly desirable for the reliability of the sensing system, [1]. Considerations on the sidelobe level such as the peak sidelobe level (PSL) and integrated sidelobe level (ISL) are main considerations for *receive* beamforming systems for which several efficient methods exist for their optimization [2,3]. Unfortunately, the power maximization requirement, which is unique to the *transmit* beamforming application, conflicts with other requirements (sidelobe suppression, flat mainlobe) and an engineering trade-off has to be made in the construction of transmit beamformers. In this paper, we examine the transmit beamforming problem under a peak-to-average power ratio (PAPR) constraint to enable such a trade-off for the design of flat-top beampatterns with low sidelobes at high power efficiency.

The problem of transmit beamforming under a PAPR constraint have been studied for the MIMO systems in the radar signal processing literature [4–9]. For instance, the waveform diversity feature allowing each antenna element to transmit independent waveforms is taken into account for the solution of transmit beamforming problem under PAPR constraint, in [5]. Several methods in the literature such as [4,5,7,10] ignore the PAPR constraint at the initial design stage and project the solution obtained without the PAPR constraint onto the set of vectors satisfying the constraint via the operation given in [11]. These methods have been shown to provide a good performance in spite of the decoupling of the problem into two stages. Different from these methods, the sequence design problem under a PAPR constraint is transformed to an unconstrained problem which can be solved via a gradient-based numerical search in [12].

The mathematical formulation of the waveform design for active sensing (transmit code design) is very similar to the transmit beamforming problem. As in transmit beamforming, the waveform

* Corresponding author.
E-mail addresses: ocayir@metu.edu.tr (Ö. Çayır), ccandan@metu.edu.tr (Ç. Candan).

https://doi.org/10.1016/j.dsp.2020.102674
1051-2004/

energy is known to be maximized with the choice of unimodular sequences for the code design problem. Unimodular sequences also maximize the achievable sensitivity by maximizing the energy incident upon and reflected from the targets [13]. Thus, the design of periodic or aperiodic unimodular sequences with low autocorrelation sidelobes is a major goal for active sensing systems, see [4, 14–19]. Since the problem of low autocorrelation sidelobes is directly related with the flatness of the spectral shape of the signal, the spectral shaping problem with unimodular sequences has been examined in several works including [15,17,20,21]. In [20], SHAPE algorithm is presented to design the sequences satisfying the temporal envelope and spectral constraints by introducing auxiliary variables. In [15], Lagrange programming neural network (LPNN) is employed to design unimodular sequences satisfying the spectral constraints. The ANSLM described in [21] minimizes the ratio of the peak stopband level to the minimum of passband level at the cost of higher ripple in the passband of the spectrum associated with a unimodular sequence.

In this study, we utilize the alternating direction method of multipliers (ADMM) for the solution of transmit beamforming problem under a PAPR constraint. ADMM is known to converge to the unique global optimum for convex problems, [22]. Yet, for nonconvex problems, it is not possible to ensure the optimality of the solution or even the convergence of the ADMM iterations. In spite of this setback, ADMM has been successfully used in many problems. In [17], unimodular sequences with low autocorrelation sidelobe are designed by ADMM after introducing auxiliary variables to separate the linear and quadratic terms of objective function and impose the nonconvex unimodularity constraint only on the linear term. Furthermore, the spectrally shaped waveform design problem is solved by ADMM via controlling the passband ripple and peak stopband level. In [19], an ADMM-based approach is proposed to solve optimization problems with nonconvex magnitude constraints for frequency/angular domains and several examples including array pattern synthesis, waveform design and robust beamforming are given to demonstrate the effectiveness of proposed method. In [18], an ADMM-based algorithm PhareADMM is presented to solve the phase retrieval problem by introducing auxiliary magnitude and phase variables to circumvent the absolute value operator in the objective function. By a simple modification exploiting the unitary property of discrete Fourier transform (DFT), PhareADMM is used to design unimodular periodic sequences having low autocorrelation sidelobe, [18]. The successful application of ADMM in many optimization problems have also initiated the generalized studies on its convergence, [23].

In this study, we use a formulation similar to the PhareADMM formulation in [18]. The main difference is the inclusion of the PAPR constraint to the problem. The inclusion of PAPR constraint requires the introduction of distinct penalty parameters for the beampattern shape and PAPR constraints. More specifically, the augmented Lagrangian function, which is the objective function minimized in primal and auxiliary variable update steps of ADMM, is defined by using distinct penalty parameters for the beampattern shape and PAPR constraints. We also suggest a simple relation to set the penalty parameters specifically for this problem. The suggested multiple penalty parameters are to control the constraint violations individually, as in [24,25], [26, pg. 292].

The main contributions are as follows:

- We examine the transmit beamformer design problem under PAPR constraint to design a flat-top beampattern with low sidelobes at a small sacrifice from the power efficiency. We use the phrase power efficiency to denote the deviation of the average transmitted power from its maximum value. The transmit power is maximized with the unimodular codes (PAPR = 1). The ratio of average transmitted power of an arbitrary weight vector to the maximum transmitted power is the power efficiency (see $P_{\text{eff}}(\mathbf{w}_\sigma)$ in Table 1).
- We formulate an ADMM-based solution with multiple penalty parameters for individually controlling the mismatches in the beampattern shape and PAPR constraints. Different from earlier approaches (finding a solution without the PAPR constraint and then projecting the solution onto a set satisfying the PAPR constraint), the suggested method generates a solution via "mixing" the optimization outputs for the spectral processing (i.e., beampattern shape) and temporal processing (i.e., PAPR constraint), where the mixture is controlled via the penalty parameters. The presented results are valid for both narrowband and wideband beamforming problems and can be extended to the waveform design problem.

Notation: Scalars, column vectors and matrices are denoted by italic lowercase, boldface lowercase and boldface uppercase letters, respectively. The real and complex fields are denoted by $\mathbb{R}$ and $\mathbb{C}$, respectively. The nonnegative orthant is denoted as $\mathbb{R}_+$, i.e., $\mathbb{R}_+ = \{a | a \in \mathbb{R}, a \geqslant 0\}$. The transpose, conjugate transpose and inverse operators are denoted by $(\cdot)^{\mathrm{T}}$, $(\cdot)^{\mathrm{H}}$ and $(\cdot)^{-1}$, respectively. The Hadamard (element-wise) product, ℓ_2-norm (Euclidean norm), absolute value and phase angle (in radians) are denoted by $\odot$, $\|\cdot\|_2$, $|\cdot|$ and $\angle(\cdot)$, respectively. The nth entry of $\mathbf{w}$ is denoted as w_n. The $\mathbb{R}^N$ ($\mathbb{C}^N$) denotes the set of the real-valued (complex-valued) N-dimensional column vectors. The $\mathbf{I}_N$ denotes the $N \times N$ identity matrix and $j = \sqrt{-1}$. The $\Re\{\cdot\}$ and $\Im\{\cdot\}$ denote the real and imaginary parts of a complex valued scalar/vector/matrix, respectively. The iteration number is denoted by parenthesized superscript.

2. System model and problem formulation

We consider a phased array system with N isotropic elements whose positions are denoted with $\mathbf{p}_n = p_{n,x}\mathbf{u}_x + p_{n,y}\mathbf{u}_y + p_{n,z}\mathbf{u}_z$, $n = 1, \ldots, N$. Here, $\mathbf{p}_n$ is a three-dimensional vector denoting the position of the nth sensor in the Cartesian coordinate system with the unit vectors of $\mathbf{u}_x$, $\mathbf{u}_y$ and $\mathbf{u}_z$.

The peak-to-average power ratio (PAPR) of the beamforming weight vector $\mathbf{w} \in \mathbb{C}^N$ is defined as

$$\text{PAPR}(\mathbf{w}) = \frac{\max\limits_{n\in\{1,\ldots,N\}} |w_n|^2}{\frac{1}{N}\sum\limits_{n=1}^{N} |w_n|^2}, \tag{1}$$

where the numerator and denominator of the ratio are the maximum and average power, respectively. It is clear that $\text{PAPR}(\cdot) : \mathbb{C}^N \to [1, N]$, where the lower bound of range corresponds to the case that all entries have the same magnitude, and the upper bound of range corresponds to the case that only one of the entries is nonzero.

For spatial processing, we take L direction samples $\{\phi_\ell, \theta_\ell\} \in [-90°, 90°]$, where ϕ_ℓ and θ_ℓ correspond to azimuth and elevation angles, respectively. Typically, we have $L \gg N$, e.g., $L \geqslant 20N$. We denote the wavenumber vector corresponding to the ℓth direction sample as

$$\mathbf{k}_\ell = 2\pi/\lambda \left(\cos\phi_\ell \cos\theta_\ell \mathbf{u}_x + \sin\phi_\ell \cos\theta_\ell \mathbf{u}_y + \sin\theta_\ell \mathbf{u}_z\right),$$

where λ is the wavelength of the transmitted signal. We form an $N \times L$ matrix $\mathbf{A}$,

$$\mathbf{A} = [\mathbf{a}_1 | \mathbf{a}_2 | \ldots | \mathbf{a}_L],$$

by concatenating the array steering vectors $\mathbf{a}_\ell \in \mathbb{C}^N$,

$$\mathbf{a}_\ell = \left[e^{j\mathbf{k}_\ell^{\mathrm{T}}\mathbf{p}_1}, e^{j\mathbf{k}_\ell^{\mathrm{T}}\mathbf{p}_2}, \ldots, e^{j\mathbf{k}_\ell^{\mathrm{T}}\mathbf{p}_N}\right]^{\mathrm{T}},$$

for $\ell = 1, \ldots, L$.

The goal is to approximate the magnitude of the desired transmit beampattern $\mathbf{b} = [b_1, \ldots, b_L]^{\mathrm{T}} \in \mathbb{R}_+^L$ by using the transmitter weight vector $\mathbf{w}$ that satisfies the PAPR constraint $\mathrm{PAPR}(\mathbf{w}) \leqslant \sigma$. It can be observed from the PAPR definition in (1) that PAPR is invariant to the scaling of $\mathbf{w}$, that is $\mathrm{PAPR}(\mathbf{w}) = \mathrm{PAPR}(c\mathbf{w})$ for any $c \in \mathbb{C}$ and $|c| \neq 0$. Hence, to disambiguate the PAPR constraint, we introduce an equality constraint $\|\mathbf{w}\|_2^2 = P$. The goal is to optimize $\mathbf{w}$ by minimizing the weighted least squares error under the PAPR constraint:

$$\begin{aligned} \underset{\mathbf{w}\in\mathbb{C}^N}{\text{minimize}} \quad & \sum_{\ell=1}^{L} h_\ell \left(b_\ell - \left|\mathbf{a}_\ell^{\mathrm{H}}\mathbf{w}\right|\right)^2 \\ \text{subject to} \quad & \mathrm{PAPR}(\mathbf{w}) \leqslant \sigma, \\ & \|\mathbf{w}\|_2^2 = P. \end{aligned} \tag{2}$$

Here $h_\ell \geqslant 0$ denotes the weight of the squared error term corresponding to the ℓth direction pair.

The main difficulties of the formulation are as follows: The term $\left|\mathbf{a}_\ell^{\mathrm{H}}\mathbf{w}\right|$ makes the objective function of (2) nondifferentiable and nonconvex. In addition, the total power constraint $\|\mathbf{w}\|_2^2 = P$ also specifies a nonconvex feasible set. Furthermore, the PAPR constraint is highly nonlinear and difficult to characterize. The PAPR constraint is examined more closely in Appendix A.

3. Proposed method

The ADMM is a distributed convex optimization method, [22]. According to [22], a well-defined projection onto nonconvex sets can also assist the convergence for nonconvex problems with a convex objective function and nonconvex constraints. Inspired by this observation, we re-express the objective function of the problem formulation in (2) so as to avoid the nonconvex magnitude function $(|\cdot|)$.

In [18], the auxiliary magnitude and phase variables are used to circumvent the magnitude operator in the objective function. We define the auxiliary variables $\alpha_\ell \in \mathbb{R}_+$ and $\beta_\ell \in \mathbb{R}$ as

$$\mathbf{a}_\ell^{\mathrm{H}}\mathbf{w} = \alpha_\ell e^{j\beta_\ell}, \tag{3}$$

where $\alpha_\ell = \left|\mathbf{a}_\ell^{\mathrm{H}}\mathbf{w}\right| \geqslant 0$ and $\beta_\ell = \angle\left(\mathbf{a}_\ell^{\mathrm{H}}\mathbf{w}\right)$ for $\ell = 1, \ldots, L$. After replacing $\left|\mathbf{a}_\ell^{\mathrm{H}}\mathbf{w}\right|$ with α_ℓ, (2) becomes

$$\begin{aligned} \underset{\substack{\mathbf{w}\in\mathbb{C}^N;\{\alpha_1,\ldots,\alpha_L\}\in\mathbb{R}_+,\\ \{\beta_1,\ldots,\beta_L\}\in\mathbb{R}}}{\text{minimize}} \quad & \sum_{\ell=1}^{L} h_\ell \left(b_\ell - \alpha_\ell\right)^2 \\ \text{subject to} \quad & \mathbf{a}_\ell^{\mathrm{H}}\mathbf{w} = \alpha_\ell e^{j\beta_\ell}, \\ & \mathrm{PAPR}(\mathbf{w}) \leqslant \sigma, \\ & \|\mathbf{w}\|_2^2 = P. \end{aligned} \tag{4}$$

Thus, in (4), the problem formulation in (2) has been converted to one with a convex objective function and nonconvex constraints.

We suggest to introduce an auxiliary vector $\mathbf{v}$ to prevent the appearance of the weight vector $\mathbf{w}$ in the PAPR constraint. With this suggestion, a solution of (4) can be generated by imposing the beampattern and PAPR constraints as the individual subproblems of ADMM:

$$\begin{aligned} \underset{\substack{\mathbf{w},\mathbf{v}\in\mathbb{C}^N;\{\alpha_1,\ldots,\alpha_L\}\in\mathbb{R}_+,\\ \{\beta_1,\ldots,\beta_L\}\in\mathbb{R}}}{\text{minimize}} \quad & \sum_{\ell=1}^{L} h_\ell \left(b_\ell - \alpha_\ell\right)^2 \\ \text{subject to} \quad & \mathbf{a}_\ell^{\mathrm{H}}\mathbf{w} = \alpha_\ell e^{j\beta_\ell}, \\ & \mathbf{w} = \mathbf{v}, \\ & \mathrm{PAPR}(\mathbf{v}) \leqslant \sigma, \\ & \|\mathbf{v}\|_2^2 = P. \end{aligned} \tag{5}$$

In (5), the beampattern shape $\{\alpha_\ell\}_{\ell=1}^L$ and $\mathrm{PAPR}(\mathbf{v})$ constraints are coupled through the equality constraint $\mathbf{w} = \mathbf{v}$.

The augmented Lagrangian for the application of ADMM on (5) requires the definition of penalty parameters. We present the augmented Lagrangian as

$$\begin{aligned} & L_{\rho_L,\rho_N}(\mathbf{w}, \boldsymbol{\alpha}, \boldsymbol{\beta}, \mathbf{v}, \mathbf{y}, \boldsymbol{\lambda}) \\ & = \sum_{\ell=1}^{L} h_\ell \left(b_\ell - \alpha_\ell\right)^2 + \sum_{\ell=1}^{L} \Re\{y_\ell\} \Re\left\{\mathbf{a}_\ell^{\mathrm{H}}\mathbf{w} - \alpha_\ell e^{j\beta_\ell}\right\} \\ & + \sum_{\ell=1}^{L} \Im\{y_\ell\} \Im\left\{\mathbf{a}_\ell^{\mathrm{H}}\mathbf{w} - \alpha_\ell e^{j\beta_\ell}\right\} + \frac{\rho_L}{2} \sum_{\ell=1}^{L} \left(\Re\left\{\mathbf{a}_\ell^{\mathrm{H}}\mathbf{w} - \alpha_\ell e^{j\beta_\ell}\right\}\right)^2 \\ & + \frac{\rho_L}{2} \sum_{\ell=1}^{L} \left(\Im\left\{\mathbf{a}_\ell^{\mathrm{H}}\mathbf{w} - \alpha_\ell e^{j\beta_\ell}\right\}\right)^2 + \sum_{n=1}^{N} \Re\{\lambda_n\} \Re\{w_n - v_n\} \\ & + \sum_{n=1}^{N} \Im\{\lambda_n\} \Im\{w_n - v_n\} + \frac{\rho_N}{2} \sum_{n=1}^{N} \left(\Re\{w_n - v_n\}\right)^2 \\ & + \frac{\rho_N}{2} \sum_{n=1}^{N} \left(\Im\{w_n - v_n\}\right)^2, \end{aligned} \tag{6}$$

where $\rho_L > 0$ and $\rho_N > 0$ are two distinct penalty parameters for beampattern shape and PAPR constraints, respectively, $\mathbf{y} = [y_1, \ldots, y_L]^{\mathrm{T}} \in \mathbb{C}^L$ and $\boldsymbol{\lambda} = [\lambda_1, \ldots, \lambda_N]^{\mathrm{T}} \in \mathbb{C}^N$ are the dual variables, $\boldsymbol{\alpha} = [\alpha_1, \ldots, \alpha_L]^{\mathrm{T}} \in \mathbb{C}^L$, $\boldsymbol{\beta} = [\beta_1, \ldots, \beta_L]^{\mathrm{T}} \in \mathbb{C}^L$ and $\mathbf{v} \in \mathbb{C}^N$ are the auxiliary variables. In (6), the real and imaginary parts are separately considered owing to the nature of ADMM, which is built on the real-valued and convex functions.

In many ADMM applications, the augmented Lagrangian functions are defined with a single penalty parameter used for all constraints [24,27,28]. However, we utilize two different penalty parameters ρ_L and ρ_N in this application. The use of a different penalty parameter for every equality constraint provides a means of individually scaling the constraint violations, as suggested in [25]. Further details on this approach can be found in [29, ch. 9].

We apply ADMM on minimizing (6) under PAPR constraint with respect to variable sets $\mathbf{w}$ and $\{\boldsymbol{\alpha}, \boldsymbol{\beta}, \mathbf{v}\}$ separately. We describe the ADMM steps involved in each iteration as follows:

Step 1: For given $\mathbf{w}^{(k)}$, $\mathbf{y}^{(k)}$ and $\boldsymbol{\lambda}^{(k)}$, the auxiliary variables at $k+1$ can be found by solving

$$\begin{aligned} & \left\{\boldsymbol{\alpha}^{(k+1)}, \boldsymbol{\beta}^{(k+1)}, \mathbf{v}^{(k+1)}\right\} = \\ & \underset{\boldsymbol{\alpha}\in\mathbb{R}_+^L, \boldsymbol{\beta}\in\mathbb{R}^L; \mathbf{v}\in\mathbb{C}^N}{\arg\min} \quad L_{\rho_L,\rho_N}(\mathbf{w}^{(k)}, \boldsymbol{\alpha}, \boldsymbol{\beta}, \mathbf{v}, \mathbf{y}^{(k)}, \boldsymbol{\lambda}^{(k)}) \\ & \text{subject to} \quad \mathrm{PAPR}(\mathbf{v}) \leqslant \sigma, \\ & \qquad\qquad\quad \|\mathbf{v}\|_2^2 = P. \end{aligned} \tag{7}$$

In the scaled form of ADMM, for $\mathbf{z} = [z_1, \ldots, z_L]^{\mathrm{T}} = \mathbf{y}/\rho_L \in \mathbb{C}^L$ and $\boldsymbol{\tau} = [\tau_1, \ldots, \tau_N]^{\mathrm{T}} = \boldsymbol{\lambda}/\rho_N \in \mathbb{C}^N$, (7) is equivalent to

$$\left\{\boldsymbol{\alpha}^{(k+1)}, \boldsymbol{\beta}^{(k+1)}, \mathbf{v}^{(k+1)}\right\}$$

$$= \underset{\substack{\boldsymbol{\alpha}\in\mathbb{R}_+^L, \boldsymbol{\beta}\in\mathbb{R}^L; \\ \mathbf{v}\in\mathbb{C}^N}}{\arg\min} \quad \sum_{\ell=1}^{L} h_\ell (b_\ell - \alpha_\ell)^2 + \frac{\rho_L}{2} \sum_{\ell=1}^{L} \left| \mathbf{a}_\ell^{\mathrm{H}} \mathbf{w}^{(k)} + z_\ell^{(k)} - \alpha_\ell e^{j\beta_\ell} \right|^2 + \frac{\rho_N}{2} \left\| \mathbf{w}^{(k)} + \boldsymbol{\tau}^{(k)} - \mathbf{v} \right\|_2^2$$

$$\text{subject to} \quad \mathrm{PAPR}(\mathbf{v}) \leqslant \sigma, \quad \|\mathbf{v}\|_2^2 = P, \tag{8}$$

as shown in Appendix B.

In (8), $\mathbf{v}$ appears only in the last term of objective function. Hence, $\mathbf{v}^{(k+1)}$ can be determined by solving the equivalent problem

$$\mathbf{v}^{(k+1)} = \underset{\mathbf{v}\in\mathbb{C}^N}{\arg\min} \quad \left\| \mathbf{w}^{(k)} + \boldsymbol{\tau}^{(k)} - \mathbf{v} \right\|_2^2 \tag{9}$$
$$\text{subject to} \quad \mathrm{PAPR}(\mathbf{v}) \leqslant \sigma, \quad \|\mathbf{v}\|_2^2 = P,$$

which is in the form of (A.1), and the solution can be found by following the steps given in [11], as discussed in Appendix A. The main role of $\mathbf{v}$ in this step is to control the PAPR of $\mathbf{w}$. By the residual convergence feature of ADMM, we should observe that the primal residual converges to zero for PAPR constraint, i.e., $\mathbf{w}^{(k)} - \mathbf{v}^{(k)} \to \mathbf{0}$ as $k \to \infty$, and hence, the PAPR and norm of $\mathbf{w}$ will be too close to that of $\mathbf{v}$ after some iterations. However, this residual convergence depends on P. Because P affects the objective function value of (9), as discussed in Appendix A.2. According to Lemma 1 of Appendix A.2, the objective function value of (9) can take zero only when $\sigma \geqslant \mathrm{PAPR}(\mathbf{w}^{(k)} + \boldsymbol{\tau}^{(k)})$ and $\|\mathbf{v}\|_2^2 = \left\|\mathbf{w}^{(k)} + \boldsymbol{\tau}^{(k)}\right\|_2^2$. As a consequence, to eliminate the possibly undesired effect of P on the residual convergence, we suggest replacing P in (9) with $\left\|\mathbf{w}^{(k)} + \boldsymbol{\tau}^{(k)}\right\|_2^2$ as follows:

$$\mathbf{v}^{(k+1)} = \underset{\mathbf{v}\in\mathbb{C}^N}{\arg\min} \quad \left\| \mathbf{w}^{(k)} + \boldsymbol{\tau}^{(k)} - \mathbf{v} \right\|_2^2 \tag{10}$$
$$\text{subject to} \quad \mathrm{PAPR}(\mathbf{v}) \leqslant \sigma, \quad \|\mathbf{v}\|_2^2 = \left\|\mathbf{w}^{(k)} + \boldsymbol{\tau}^{(k)}\right\|_2^2.$$

It is clear that the feasible set of (10) varies with k unlike that of (9). Hence, $\mathbf{w}^{(k)}$ can converge to a point which is not feasible for (2) due to violation of total power constraint, e.g., $\left\|\mathbf{w}^{(k)}\right\|_2^2 \neq P$, when $\mathbf{w}^{(k)} - \mathbf{v}^{(k)} \to \mathbf{0}$ as $k \to \infty$. By scaling $\mathbf{w}^{(k)}$, we can obtain a point $\sqrt{P}\,\mathbf{w}^{(k)} / \left\|\mathbf{w}^{(k)}\right\|_2$ satisfying the total power constraint of (2). As seen from the PAPR definition in (1), the scaling of a vector does not change its PAPR, and we have $\mathrm{PAPR}(\sqrt{P}\mathbf{w}^{(k)} / \left\|\mathbf{w}^{(k)}\right\|_2) = \mathrm{PAPR}(\mathbf{w}^{(k)})$. Moreover, after the scaling, only the transmit beampattern shape is shifted up or down in dB scale and the performance metrics such as PSL and mainlobe ripple are not affected.

Similarly, $\boldsymbol{\beta}$ appears only in the middle term of the objective function of (8), and the equivalent problem for determining $\boldsymbol{\beta}^{(k+1)}$ is

$$\boldsymbol{\beta}^{(k+1)} = \underset{\boldsymbol{\alpha}\in\mathbb{R}_+^L, \boldsymbol{\beta}\in\mathbb{R}^L}{\arg\min} \left(\sum_{\ell=1}^{L} \left| \mathbf{a}_\ell^{\mathrm{H}} \mathbf{w}^{(k)} + z_\ell^{(k)} - \alpha_\ell e^{j\beta_\ell} \right|^2 \right). \tag{11}$$

Let $\boldsymbol{\gamma} = [\gamma_1, \ldots, \gamma_L]^{\mathrm{T}} \in \mathbb{C}^L$, where $\gamma_\ell = \alpha_\ell e^{j\beta_\ell}$ for $\ell = 1, \ldots, L$. Then, the objective function of (11) can be expressed as

$$\sum_{\ell=1}^{L} \left| \mathbf{a}_\ell^{\mathrm{H}} \mathbf{w}^{(k)} + z_\ell^{(k)} - \alpha_\ell e^{j\beta_\ell} \right|^2 = \left\| \mathbf{A}^{\mathrm{H}} \mathbf{w}^{(k)} + \mathbf{z}^{(k)} - \boldsymbol{\gamma} \right\|_2^2. \tag{12}$$

As $\boldsymbol{\beta} = \angle \boldsymbol{\gamma}$, the solution of (11) is found as

$$\boldsymbol{\beta}^{(k+1)} = \angle \left(\mathbf{A}^{\mathrm{H}} \mathbf{w}^{(k)} + \mathbf{z}^{(k)} \right), \tag{13}$$

where $\mathbf{A} = [\mathbf{a}_1 | \mathbf{a}_2 | \ldots | \mathbf{a}_L] \in \mathbb{C}^{N\times L}$.

Replacing β_ℓ with $\beta_\ell^{(k+1)}$ in the objective function of (8), we obtain the equivalent problem to find $\boldsymbol{\alpha}^{(k+1)}$ as follows:

$$\boldsymbol{\alpha}^{(k+1)} = \underset{\boldsymbol{\alpha}\in\mathbb{R}_+^L}{\arg\min} \left(\sum_{\ell=1}^{L} h_\ell \left(b_\ell - \alpha_\ell\right)^2 + \frac{\rho_L}{2} \sum_{\ell=1}^{L} \left(r_\ell - \alpha_\ell\right)^2 \right), \tag{14}$$

where $r_\ell = \left| \mathbf{a}_\ell^{\mathrm{H}} \mathbf{w}^{(k)} + z_\ell^{(k)} \right|$ for $\ell = 1, \ldots, L$.

Taking the derivative of the objective function in (14) with respect to α_ℓ and zeroing at $\alpha_\ell^{(k+1)}$, we get

$$0 = 2h_\ell b_\ell - 2h_\ell \alpha_\ell^{(k+1)} + \rho_L r_\ell - \rho_L \alpha_\ell^{(k+1)}.$$

Since α_ℓ denotes the magnitude, i.e., $\alpha_\ell \geqslant 0$, the solution is given as follows:

$$\alpha_\ell^{(k+1)} = \begin{cases} \dfrac{\rho_L r_\ell + 2h_\ell b_\ell}{\rho_L + 2h_\ell}, & \dfrac{\rho_L r_\ell + 2h_\ell b_\ell}{\rho_L + 2h_\ell} \geqslant 0 \text{ and} \\ & \rho_L + 2h_\ell \neq 0 \\ 0, & \text{otherwise} \end{cases} \tag{15}$$

for $\ell = 1, \ldots, L$.

For our application, $\rho_L > 0$, $r_\ell \geqslant 0$, $h_\ell \geqslant 0$ and $b_\ell \geqslant 0$ satisfy that $\rho_L r_\ell + 2h_\ell b_\ell \geqslant 0$ and $\rho_L + 2h_\ell > 0$, and hence, (15) can be simplified as

$$\alpha_\ell^{(k+1)} = \frac{\rho_L r_\ell + 2h_\ell b_\ell}{\rho_L + 2h_\ell} \tag{16}$$

for $\ell = 1, \ldots, L$.

Step 2: We update $\mathbf{w}$ by solving

$$\mathbf{w}^{(k+1)} = \underset{\mathbf{w}\in\mathbb{C}^N}{\arg\min}\, L_{\rho_L,\rho_N}(\mathbf{w}, \boldsymbol{\alpha}^{(k+1)}, \boldsymbol{\beta}^{(k+1)}, \mathbf{v}^{(k+1)}, \mathbf{z}^{(k)}, \boldsymbol{\tau}^{(k)}). \tag{17}$$

According to (17), all variables except $\mathbf{w}$ are fixed in (6). Thus, the objective function of (8) that is modified from (6) due to the fixed $\mathbf{z}^{(k)}$ and $\boldsymbol{\tau}^{(k)}$ can be manipulated further by using the fixed $\boldsymbol{\gamma}^{(k+1)} = \boldsymbol{\alpha}^{(k+1)} \odot e^{j\boldsymbol{\beta}^{(k+1)}}$, as in (12). Then, (17) is equivalent to

$$\mathbf{w}^{(k+1)} = \underset{\mathbf{w}\in\mathbb{C}^N}{\arg\min} \left(\left\| \mathbf{A}^{\mathrm{H}} \mathbf{w} + \mathbf{z}^{(k)} - \boldsymbol{\gamma}^{(k+1)} \right\|_2^2 + \frac{\rho_N}{\rho_L} \left\| \mathbf{w} + \boldsymbol{\tau}^{(k)} - \mathbf{v}^{(k+1)} \right\|_2^2 \right), \tag{18}$$

which is quadratic in $\mathbf{w}$. Setting gradient of the objective function in (18) equal to zero for $\mathbf{w}^{(k+1)}$ [30], we get

$$0 = \mathbf{A} \left(\mathbf{A}^{\mathrm{H}} \mathbf{w}^{(k+1)} + \mathbf{z}^{(k)} - \boldsymbol{\gamma}^{(k+1)} \right) + \frac{\rho_N}{\rho_L} \left(\mathbf{w}^{(k+1)} + \boldsymbol{\tau}^{(k)} - \mathbf{v}^{(k+1)} \right),$$

and find

$$\mathbf{w}^{(k+1)} = \left(\mathbf{A}\mathbf{A}^{\mathrm{H}} + \frac{\rho_N}{\rho_L} \mathbf{I}_N \right)^{-1} \left(\mathbf{A} \left(\boldsymbol{\gamma}^{(k+1)} - \mathbf{z}^{(k)} \right) + \frac{\rho_N}{\rho_L} \left(\mathbf{v}^{(k+1)} - \boldsymbol{\tau}^{(k)} \right) \right). \tag{19}$$

Step 3: The dual updates are

$$\mathbf{z}^{(k+1)} = \mathbf{z}^{(k)} + \mathbf{A}^{\mathrm{H}} \mathbf{w}^{(k+1)} - \boldsymbol{\gamma}^{(k+1)}, \tag{20}$$

$$\boldsymbol{\tau}^{(k+1)} = \boldsymbol{\tau}^{(k)} + \mathbf{w}^{(k+1)} - \mathbf{v}^{(k+1)}. \tag{21}$$

Algorithm 1 PAPR-ADMM, algorithm for computing the transmitter weights having PAPR between 1 and σ, also see [31].

Input: $\mathbf{w}^{(1)}$, $\mathbf{A}$, $\mathbf{b}$, $\mathbf{h}$, ρ_L, σ, P and $k_{\max}$
Initialization: $\mathbf{w}^{(0)} = 2\mathbf{w}^{(1)}$, $\mathbf{y}^{(1)} = \mathbf{0}$, $\boldsymbol{\lambda}^{(1)} = \mathbf{0}$, and $k = 1$
  compute ρ_N from (22)
  compute $\mathbf{z}^{(1)} = \mathbf{y}^{(1)}/\rho_L$ and $\boldsymbol{\tau}^{(1)} = \boldsymbol{\lambda}^{(1)}/\rho_N$
  while $k \leqslant k_{\max}$ and $\left\|\mathbf{w}^{(k)} - \mathbf{w}^{(k-1)}\right\|_2 > 10^{-6}\left\|\mathbf{w}^{(k-1)}\right\|_2$ **do**
    // Step-1
    compute $\mathbf{v}^{(k+1)}$ from (10)
    compute $\boldsymbol{\beta}^{(k+1)}$ from (13)
    compute $\boldsymbol{\alpha}^{(k+1)}$ from (16)
    form $\boldsymbol{\gamma}^{(k+1)}$, where $\gamma_\ell = \alpha_\ell e^{j\beta_\ell}$, $\ell = 1, \ldots, L$
    // Step-2
    compute $\mathbf{w}^{(k+1)}$ from (19)
    // Step-3
    compute $\mathbf{z}^{(k+1)}$ from (20)
    compute $\boldsymbol{\tau}^{(k+1)}$ from (21)
    $k = k + 1$
  end while
  assign $\mathbf{w}^f = \mathbf{w}^{(k+1)}$
  compute $\mathbf{w}^\star$ from (23)
  return $\mathbf{w}^\star$

We have described the steps to compute the transmitter weights satisfying the PAPR constraint. Then, we have a suggestion for penalty parameters selection. The suggested method has two distinct penalty parameters ρ_L and ρ_N, and they are jointly used only in (19). To keep a balance between $\mathbf{A}(\boldsymbol{\gamma}^{(k+1)} - \mathbf{z}^{(k)})$ and $\rho_N/\rho_L\left(\mathbf{v}^{(k+1)} - \boldsymbol{\tau}^{(k)}\right)$ in (19), we suggest $\rho_N/\rho_L = \|\mathbf{A}\|_2$ which is also equal to the largest singular value of $\mathbf{A}$. Hence, ρ_N can be set as

$$\rho_N = \rho_L \|\mathbf{A}\|_2. \tag{22}$$

The suggested method is referred to as PAPR-ADMM and is outlined in Algorithm 1. The PAPR-ADMM requires an initial condition vector $\mathbf{w}^{(1)} \in \mathbb{C}^N$, which can be a unimodular vector for the transmit beamforming application. After initializing dual variables as $\mathbf{y}^{(1)} = \mathbf{0}$, $\boldsymbol{\lambda}^{(1)} = \mathbf{0}$, the steps described in this section are iteratively applied until the condition

$$\frac{\left\|\mathbf{w}^{(k)} - \mathbf{w}^{(k-1)}\right\|_2}{\left\|\mathbf{w}^{(k-1)}\right\|_2} \leqslant 10^{-6}$$

or the maximum iteration number $k = k_{\max}$ is satisfied. Note that after the final iteration, $\mathrm{PAPR}(\mathbf{w}^{(k+1)}) \leqslant \sigma$ may not hold due to the update equation (19). The final transmitter weights $\mathbf{w}^f$ after termination of iterations may require an adjustment to meet the PAPR constraint of (2). We suggest to implement the PAPR update again on $\mathbf{w}^f$:

$$\begin{aligned} \mathbf{w}^\star = \underset{\mathbf{w}\in\mathbb{C}^N}{\arg\min} \quad & \left\|\mathbf{w}^f - \mathbf{w}\right\|_2^2 \\ \text{subject to} \quad & \mathrm{PAPR}(\mathbf{w}) \leqslant \sigma, \\ & \|\mathbf{w}\|_2^2 = P. \end{aligned} \tag{23}$$

Note that $\mathbf{w}^\star$ is simply the Euclidean projection of $\mathbf{w}^f$ onto the feasible set of (2) that is given by [11].

Conventionally ADMM is built on the real-valued and convex functions. In this study, we have given the formulation by separating the real and imaginary parts of complex variables, see (6). Then, we have utilized the complex-valued vector-matrix calculations to get an equivalent form, see the primal and dual updates. Depending on the application, e.g., when $\mathbf{A}^{\mathrm{H}}\mathbf{w}$ is the DFT of $\mathbf{w}$, we can apply DFT and inverse DFT and simplify the matrix inverse calculation in (19).

Next, we present an extension of the formulation to the wideband transmit beamformer design.

3.1. Wideband beamforming

In wideband beamforming, the goal is to set the sensor weights that give the desired beampattern within the negligible difference for different operating frequencies/wavelengths. The wavelengths of interest correspond a limited bandwidth around the center frequency of the transmitter. Considering the well known quality factor definition,

$$Q_f = \frac{f_c}{\Delta_f}, \tag{24}$$

where f_c is the center frequency, Δ_f is the bandwidth of the transmitting elements for the definition of frequency samples $f_i \in \left[f_c - \Delta_f/2, f_c + \Delta_f/2\right]$, we can express the matrix $\mathbf{A}_i$, as in Section 2, for each frequency sample $i = 1, \ldots, F$. Concatenating $\mathbf{A}_i$ matrices, we define

$$\mathbf{A}_{\mathrm{wb}} \triangleq [\mathbf{A}_1 | \mathbf{A}_2 | \ldots | \mathbf{A}_F],$$

which is an $N \times FL$ matrix of array steering vectors. Similarly, we can obtain the desired beampattern vector $\mathbf{b}_{\mathrm{wb}} \in \mathbb{R}_+^{FL}$ by concatenating the desired beampatterns for frequency samples.

Thus, the wideband beamforming problem with PAPR constraint is given as

$$\begin{aligned} \underset{\mathbf{w}\in\mathbb{C}^N}{\text{minimize}} \quad & \sum_{\ell=1}^{FL} h_\ell \left(b_\ell - \left|\mathbf{a}_\ell^{\mathrm{H}}\mathbf{w}\right|\right)^2 \\ \text{subject to} \quad & \mathrm{PAPR}(\mathbf{w}) \leqslant \sigma, \\ & \|\mathbf{w}\|_2^2 = P, \end{aligned} \tag{25}$$

where $\mathbf{a}_\ell$ is the ℓth column of $\mathbf{A}_{\mathrm{wb}}$, b_ℓ is the ℓth entry of $\mathbf{b}_{\mathrm{wb}}$, and $h_\ell \geqslant 0$ is the weight of the squared error term corresponding to the ℓth direction pair for $\ell = 1, \ldots, FL$. This problem has the form of (2), and it can be solved simply by replacing $\mathbf{A}$ and $\mathbf{b}$ in Algorithm 1 with $\mathbf{A}_{\mathrm{wb}}$ and $\mathbf{b}_{\mathrm{wb}}$, respectively.

3.2. Algorithm convergence

The convergence of ADMM for nonconvex problems is an important theoretic problem of the optimization literature, [23]. Algorithm convergence depends on the initial primal and dual points, the penalty parameter and also on the formulation of update steps, [22]. Unfortunately, the PAPR constraint (due to its nonlinearity) does not lend itself to further analysis. In our experience, PAPR-ADMM with the suggested settings has converged at all runs that we have implemented. The main difficulty that we face is not the convergence, the need of running PAPR-ADMM repeatedly with different initial conditions to avoid local optima. The sensitivity to the initial conditions is expected given the multimodal nature of the beampattern matching problem, as discussed in [5]. To improve the performance, we suggest to use the formulation (10) instead of (9) and examine this suggestion with some common parameter settings in Section 4. Readers are also invited to conduct Monte-Carlo trials of PAPR-ADMM with randomized initial conditions by running a ready-to-use MATLAB code at [31].

3.3. Computational complexity considerations

We are able to present closed-form expressions for the solution of all steps in Algorithm 1 except (10) and (23), which is provided in [11]. Equations (10) and (23) have the form of (A.1) that requires a sorting operation with the complexity of $\mathcal{O}(N \log N)$ operations and a processing of a vector with the worst case computational complexity of $\mathcal{O}(N^2)$. Here, (10) is evaluated in Step-1 of each

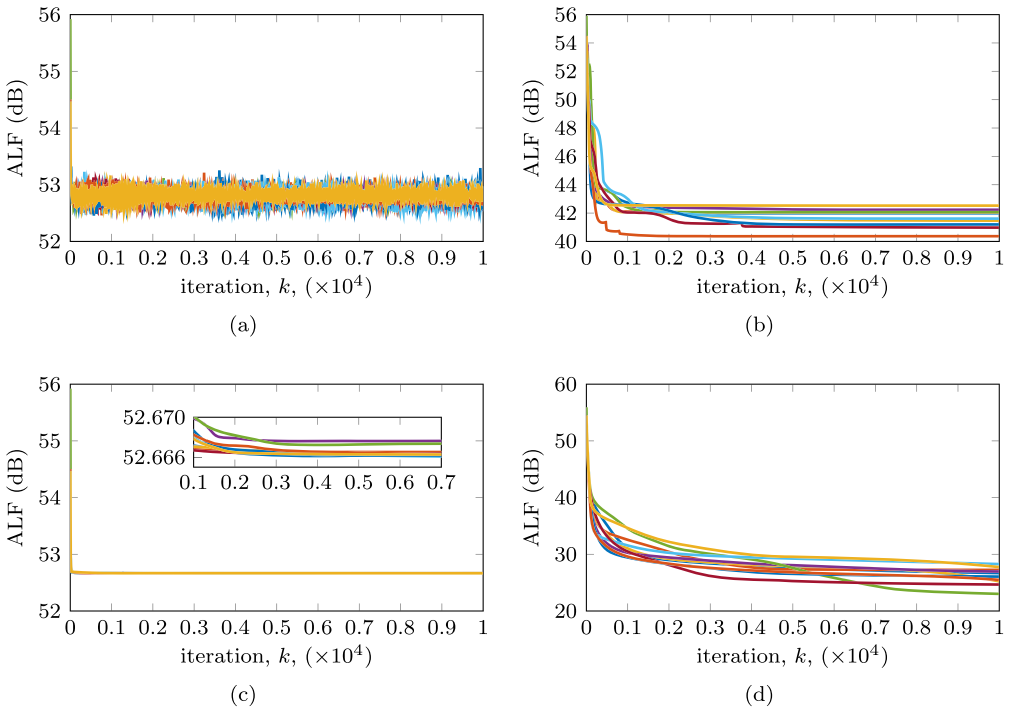

Fig. 1. For narrowband transmit beamforming with 32 elements ULA, the augmented Lagrangian function (6) versus iteration number, $L_{\rho_L,\rho_N}(\mathbf{w}^{(k)},\boldsymbol{\alpha}^{(k)},\boldsymbol{\beta}^{(k)},\mathbf{v}^{(k)},\mathbf{y}^{(k)},\boldsymbol{\lambda}^{(k)})$: (a) PAPR = 1 using (9), (b) PAPR = 1 using (10), (c) PAPR = 2 using (9), and (d) PAPR = 2 using (10).

iteration, whereas (23) is evaluated once after the termination of iterations.

In Step-1 of Algorithm 1, the required updates are implemented through the equations (13) and (16) requiring $\mathcal{O}(LN)$ multiplications. In Step-2, (19) requires $\mathcal{O}\left(LN^2\right)$. In Step-3, (20) and (21) require $\mathcal{O}(LN)$ and $\mathcal{O}(N)$, respectively. Therefore, the computational complexity of each iteration is $\mathcal{O}\left(LN^2\right)$, which can be reduced further by computing the matrix inverse in (19) offline and storing the result. With the storage option, the computational complexity of Step-2 is reduced to $\mathcal{O}\left(N^2\right)$, and the overall complexity of each iteration becomes $\mathcal{O}\left(N^2+LN\right)$ multiplications.

4. Numerical comparisons

Unless otherwise is stated, we set $\rho_L = 25$, $k_{\max} = 10000$, $\mathbf{h} = [h_1,\ldots,h_L]^{\mathrm{T}}$ is constructed with $h_\ell = \delta_{\mathrm{m}}$ if the ℓth direction sample corresponds to the mainlobe (or passband), and $h_\ell = \delta_{\mathrm{s}}$ otherwise, where $\delta_{\mathrm{s}}/\delta_{\mathrm{m}} = 100$. Initial condition weight vector is set as $\mathbf{w}^{(1)} = \left[w_1^{(1)}, w_2^{(1)},\ldots,w_N^{(1)}\right]^{\mathrm{T}}$, where $w_n^{(1)} = e^{j2\pi\mu_n}$ for $n = 1,\ldots,N$ and $\mu_1,\ldots,\mu_N$ are i.i.d. random variables uniformly distributed on $(0,1)$.

We assume a sonar system having $N = 32$ elements uniform linear array (ULA). The distance between neighboring sensors is $\lambda/2$ for the center frequency 150 kHz, where λ is determined by using the speed of sound in water, which is taken as 1500 m/s.

4.1. Effect of fixed total power

Our goal is to study the algorithm performance when (9) is utilized instead of (10) in Step-1. We have 10 realizations for the initial weight vector. For each realization, we apply PAPR-ADMM by setting PAPR, $\sigma \in S_\sigma = \{1, 2\}$, and $P = N$ with the formulation given by (9) (fixed total power), or (10) (varying total power). In Fig. 1, the augmented Lagrangian function (ALF) value (6) versus iteration number k is shown. Comparing Fig. 1(a) and (b), we notice that the fixed total power formulation prevents the monotonicity of ALF when PAPR = 1. For PAPR = 2, both formulations provide the monotonous ALF values after some iterations, as shown in Fig. 1(c) and (d). Hence, we suggest the usage of formulation (10) in Step-1 of Algorithm 1 for the performance improvement.

4.2. Mainlobe average power versus PAPR

We consider the sonar system given for the previous experiment. Setting PAPR, $\sigma \in S_\sigma = \{1, 1.01, 1.02, 1.03, 1.04, 1.05, 1.1, 1.2, 1.25, 1.3, 1.4, 1.5, 1.6, 1.7, 1.75, 1.8, 1.9, 2, 3, 4, 5, 6\}$, we design a 1-D flat-top beampattern by using PAPR-ADMM initialized with the same initial vector $\mathbf{w}^{(1)}$. The PSL of the desired beampattern is 30 dB. The mainlobe is centered at $(0°, 0°)$ in (azimuth, elevation). The desired half-beamwidth and transition width are 45° and 8° in azimuth, respectively. The direction samples are taken by using a uniform grid spacing of 0.1°.

The experiment is conducted to observe the mainlobe average power versus PAPR for narrowband transmit beamforming. As a strategy for maximizing the total transmitted power, transmitter weights are normalized so that the peak (or maximum) power is always fixed to the maximum allowed power that can be transmitted from an antenna. Thus, each weight $\mathbf{w}_\sigma$ for $\sigma \in S_\sigma$ is scaled to have entries with the maximum magnitude of 1 before computing the mainlobe average power. Consequently, the numerator of (1) is fixed to 1 for each $\mathbf{w}_\sigma$, and only $\|\mathbf{w}_\sigma\|_2^2$ is affected from the changed σ. Owing to the power conservation, we increase the average power of the designed beampattern by increasing $\|\mathbf{w}_\sigma\|_2^2$. Our method actually solves a constrained LS problem by trying to keep the ratio of the average power in mainlobe and sidelobe at some level. Hence, we observe that the mainlobe average power is decreased when PAPR($\mathbf{w}_\sigma$) is increased, as shown in Fig. 2. Owing to the same initial point, we can observe the achievable PAPR to which PAPR($\mathbf{w}_\sigma$) converges. This value is less than 5 for our parameters and initial point, and the results are not affected any more if we increase σ from 5 to 6.

For some PAPR values, the performance metrics of the designed beampatterns are given in Table 1, where $P_{\mathrm{avg}}^{\mathrm{m}}$ is the mainlobe av-

Table 1
Performance Metrics for Narrowband Transmit Beamforming with 32 Elements ULA and PAPR $\leqslant \sigma$.

σ	1	1.01	1.02	1.05	1.4	1.6	1.75	1.9	2	3	4	5, 6
$P^{\mathrm{m}}_{\mathrm{avg}}$ (dB)	16.3609	16.3205	16.2850	16.2237	14.9758	14.3975	13.9638	13.5994	13.3865	11.6160	10.3677	9.6810
$P^{\mathrm{m}}_{\mathrm{p\text{-}p}}$ (dB)	9.7083	8.8528	8.5463	7.6724	3.6882	1.9813	1.0921	0.6956	0.5755	0.5489	0.5364	0.5470
PSL (dB)	19.9537	21.6018	21.7920	22.4198	24.1667	26.5034	27.3493	27.6373	28.7691	28.8939	28.6532	28.7207
PAPR($\mathbf{w}_\sigma$)	1	1.01	1.02	1.05	1.4	1.6	1.75	1.9	2	3	4	4.6884
$P_{\mathrm{eff}}(\mathbf{w}_\sigma)$ (%)	100.00	99.01	98.04	95.24	71.43	62.50	57.14	52.63	50.00	33.33	25.00	21.33
$P^{\mathrm{m}}_{\mathrm{min}}$ (dB)	9.9636	10.8448	11.1819	11.8114	12.5919	13.3165	13.3591	13.2474	13.0861	11.2791	9.9710	9.2830
$P^{\mathrm{m}}_{\mathrm{max}}$ (dB)	19.6719	19.6976	19.7282	19.4837	16.2801	15.2978	14.4512	13.9430	13.6616	11.8280	10.5074	9.8300
$P^{\mathrm{s}}_{\mathrm{avg}}$ (dB)	−13.164	−13.295	−13.535	−13.620	−14.898	−15.525	−16.010	−16.385	−16.608	−18.382	−19.631	−20.318
$P^{\mathrm{m/s}}_{\mathrm{avg}}$ (dB)	29.5250	29.6155	29.8201	29.8441	29.8736	29.9225	29.9742	29.9845	29.9943	29.9984	29.9992	29.9993
R_{max} (%)	100.00	99.77	99.56	99.21	92.34	89.31	87.11	85.30	84.26	76.10	70.82	68.08

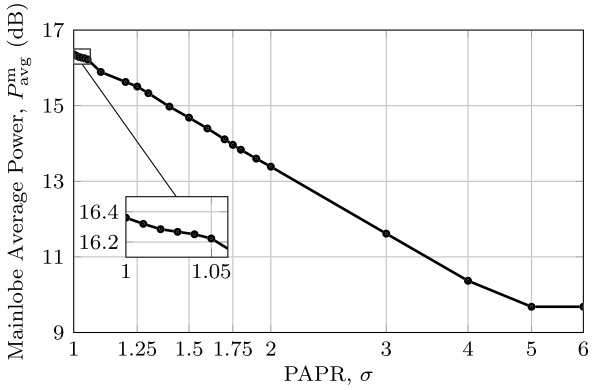

Fig. 2. For narrowband transmit beamforming with 32 elements ULA, mainlobe average power versus PAPR (base-2 log scale is used for the PAPR axis).

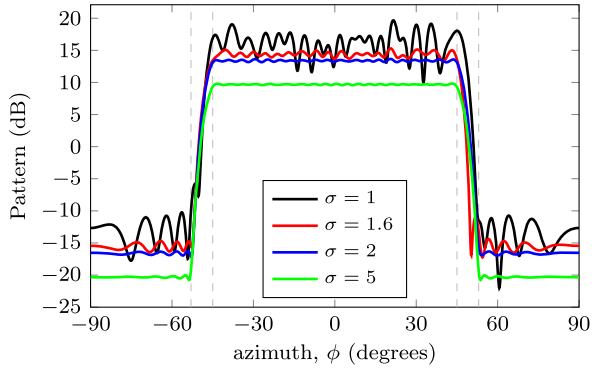

Fig. 3. For narrowband transmit beamforming with 32 elements ULA, beampattern versus PAPR.

erage power, $P^{\mathrm{m}}_{\mathrm{p\text{-}p}}$ is the peak-to-peak power variation in mainlobe, $P_{\mathrm{eff}}(\mathbf{w}_\sigma) = 100 \cdot \|\mathbf{w}_\sigma\|_2^2 / \|\mathbf{w}_1\|_2^2$ is the power efficiency, $P^{\mathrm{m}}_{\mathrm{min}}$ is the minimum and $P^{\mathrm{m}}_{\mathrm{max}}$ is the maximum power in mainlobe, $P^{\mathrm{s}}_{\mathrm{avg}}$ is the sidelobe average power, $P^{\mathrm{m/s}}_{\mathrm{avg}}$ is the ratio of the average power in mainlobe and sidelobe, see Appendix C for the computation of average power, and R_{max} is the maximum range ratio defined as

$$(R_{\mathrm{max}})_\sigma = 100 \cdot \left(\frac{(P^{\mathrm{m}}_{\mathrm{avg}})_\sigma}{(P^{\mathrm{m}}_{\mathrm{avg}})_1} \right)^{1/4}$$

by using the relation that the maximum range is proportional to (average power $\times$ aperture)$^{1/4}$ [1].

The beampatterns corresponding to $\sigma \in \{1, 1.6, 2, 5\}$ are shown in Fig. 3. As a comparison, $\sigma = 1$ design (PAPR $= 1$ case) presents maximum average power over the illuminated sector ($P^{\mathrm{m}}_{\mathrm{avg}} = 16.3609$ dB) at the expense of large peak-to-peak power swing ($P^{\mathrm{m}}_{\mathrm{p\text{-}p}} = 9.7083$ dB). While $\sigma = 1.6$ design has about 2 dB less average power in the mainlobe ($P^{\mathrm{m}}_{\mathrm{avg}} = 14.3975$ dB), yet has a peak-to-peak power swing of 1.9813 dB in the mainlobe. Furthermore, $\sigma = 1.6$ design has a better PSL than $\sigma = 1$ design by 6.5 dB. On the other extreme, when PAPR constraint is ignored, which the case of $\sigma = 5$ or $\sigma = 6$; power swing in the mainlobe is minimized to 0.5470 dB and PSL is improved 28.7207 dB, yet the average power over the illuminated region is only 9.6810 dB which is about a quarter of $\sigma = 1$ design. The maximum range is decreased to 89.31% (about 10% range loss) and 68.08 (about 30% range loss) for $\sigma = 1.6$ and $\sigma = 5$ (or $\sigma = 6$) design, respectively.

As noted previously, the goal of the present study is to let the designer trade-off between several metrics, as shown in Table 1, with a proper choice of PAPR value.

4.3. Radar waveform design with unimodular sequence

The second experiment is related to a radar application, where a unimodular periodic sequence is required to communicate through a crowded channel. While the beamforming applications are our main concern, we also give this example to put forward the feasibility of the method in other applications.

Table 2
Comparison of Peak-to-Peak Power Variation in Passband and PSL Values for Radar Waveform Design.

Method	SHAPE [20]	LPNN [15]	ADMM [17]	PAPR-ADMM
$P^{\mathrm{m}}_{\mathrm{p\text{-}p}}$ (dB)	2.7351	9.9479	1.7607	1.4021
PSL (dB)	15.1515	13.5066	19.0311	19.2167

We compare the proposed method PAPR-ADMM with the unimodular sequence design methods SHAPE [20], LPNN [15], ADMM [17] for radar waveform design experiment described in [17]. The radar has the sample rate 810 kHz and the pulse duration 200 µs, and therefore, the sequence length is $N = 162$. With respect to the normalized frequency, the stopband intervals are $[0, 0.0617]$, $[0.0988, 0.2469]$, $[0.2593, 0.2840]$, $[0.3086, 0.3827]$, $[0.4074, 0.4938]$, $[0.5185, 0.5556]$, and $[0.9383, 1.0000]$, and the rest of intervals correspond to the passband. The SHAPE[1] and ADMM require upper and lower masks for passband specified by the ripple constraint 0.2, whereas LPNN and PAPR-ADMM require the unity passband mask. The peak stopband level is $\eta = 0.01$ or $\eta = -20$ dB. The spectrum of each sequence is shown in Fig. 4, and the corresponding peak-to-peak power variation in passband, $P^{\mathrm{m}}_{\mathrm{p\text{-}p}}$, and PSL values are given in Table 2. Each sequence has comparable autocorrelation sidelobe levels, as shown in Fig. 5.

Next, we compare our method with ANSLM [21]. For PAPR-ADMM, $\eta = -29$ dB, and the ratio of stopband and passband sample weights is $\delta_{\mathrm{s}}/\delta_{\mathrm{m}} = 1000$ to increase the power variation in passband. The spectra of sequences designed by using ANSLM and PAPR-ADMM are shown in Fig. 6. For ANSLM, PSL and $P^{\mathrm{m}}_{\mathrm{p\text{-}p}}$ values are 24.1653 dB and 9.2059 dB, respectively. With PAPR-ADMM, we

[1] MATLAB code is available on www.sal.ufl.edu/shape.

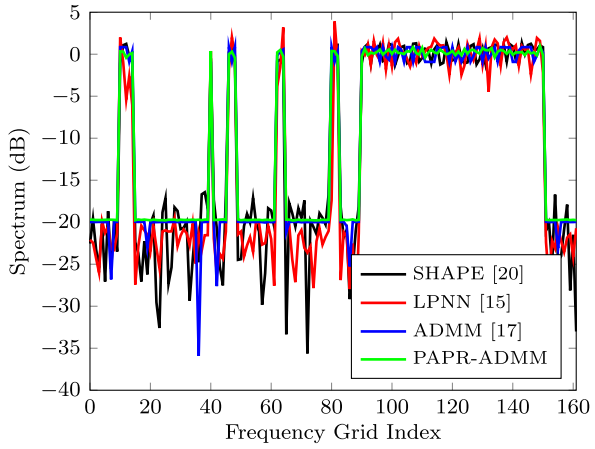

Fig. 4. Comparison of spectra for radar waveform design with $\eta = -20$ dB.

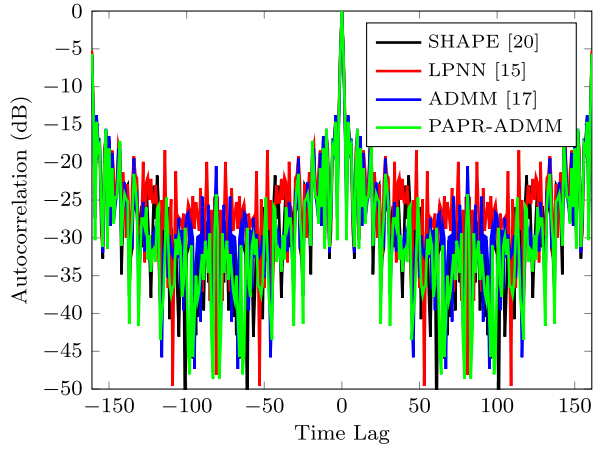

Fig. 5. Comparison of autocorrelation functions for radar waveform design with $\eta = -20$ dB.

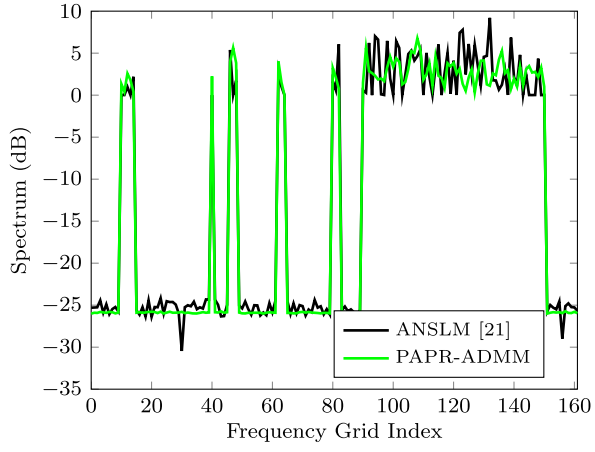

Fig. 6. Comparison of spectra for radar waveform design with ANSLM.

observe PSL as 25.7239 dB and $P^{\text{m}}_{\text{p-p}}$ as 6.7645 dB. Both sequences have comparable autocorrelation sidelobe levels, as shown in Fig. 7.

4.4. Wideband transmit beamforming

We consider a sonar system having $N = 144$ elements uniform rectangular array (URA). The distance between neighboring sensors is $\lambda/2$ for 150 kHz with the propagation speed of 1500 m/s. For wideband beamforming, the center frequency f_c is 140 kHz and

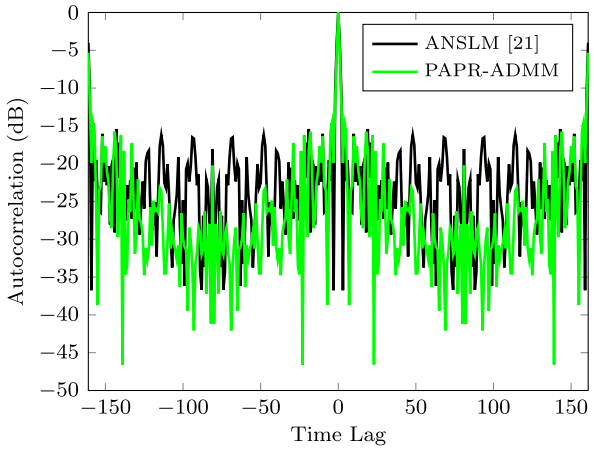

Fig. 7. Comparison of autocorrelation functions for radar waveform design with ANSLM.

the quality factor Q_f is 14. Using (24), we compute Δ_f as 10 kHz. Then, we take frequency sample $f_i \in \{135, 137.5, 140, 142.5, 145\}$ kHz for $i = 1, \ldots, 5$. Setting PAPR, $\sigma \in S_\sigma = \{1, 2, 8, 36\}$, and using PAPR-ADMM initialized with the same vector $\mathbf{w}^{(1)}$, we find the transmitter weights $\mathbf{w}_\sigma$ that can be used to compute the 2-D flat-top beampatterns corresponding to these frequencies. The PSL of the desired beampattern is 15 dB. The mainlobe is inside of an elliptical region centered at $(0°, 0°)$ and having semi-major and semi-minor axis of 35° and 15°, respectively. The sidelobe is outside of an elliptical region centered at $(0°, 0°)$ and having semi-major and semi-minor axis of 43° and 20°, respectively. The direction samples are taken by using a uniform grid spacing of 1°. Since the array has uniform grid and the desired beampattern is symmetric in azimuth and elevation, we can assume that the transmitter weights are symmetric in horizontal and vertical directions. Therefore, we decrease the search space dimension from 144 to 36 and set σ as 36 at most.

The beampatterns on cutting-planes, i.e., $(\phi, 0°)$ and $(0°, \theta)$ planes, are shown in Fig. 8. For $\sigma \in \{1, 2\}$, the mainlobe has higher ripple than that of beampatterns corresponding to $\sigma \in \{8, 36\}$. The maximum of achievable PAPR is observed as $\text{PAPR}(\mathbf{w}_\sigma) = 12.3071$ for $\sigma = 36$.

5. Summary and conclusions

The main goal of the study is to examine the transmit beamformer design problem under the peak-to-average-power-ratio (PAPR) constraint. The PAPR constraint is included in the problem setting to provide a trade-off mechanism between the beampattern shape, average power in the mainlobe and other classical metrics such as PSL, ISL, etc. Typically, a flat-top beampattern and maximum average power transmission over the sector of interest are jointly desired. Unfortunately, these two objectives are contradictory and the introduced PAPR constraint provides a mean of trading one objective with the other. For example, the choice of $\text{PAPR} = 1$ (unimodular transmitter weight design) maximizes the average transmitted power in the mainlobe at the expense of severe power fluctuations in the mainlobe, low PSL values, etc. For the example in Table 1, relaxing the PAPR constraint to 1.6 improves the mainlobe power fluctuations by about 8 dB, PSL about 6.5 dB at the expense of 2 dB less average power transmission in the mainlobe. At the other extreme, setting $\text{PAPR} = N$, where N is the number of the transmitting elements, corresponds to a design problem without a PAPR constraint. Such a choice is suitable for the receive beamforming where the average power in the mainlobe region is not a concern at all. For the solution of

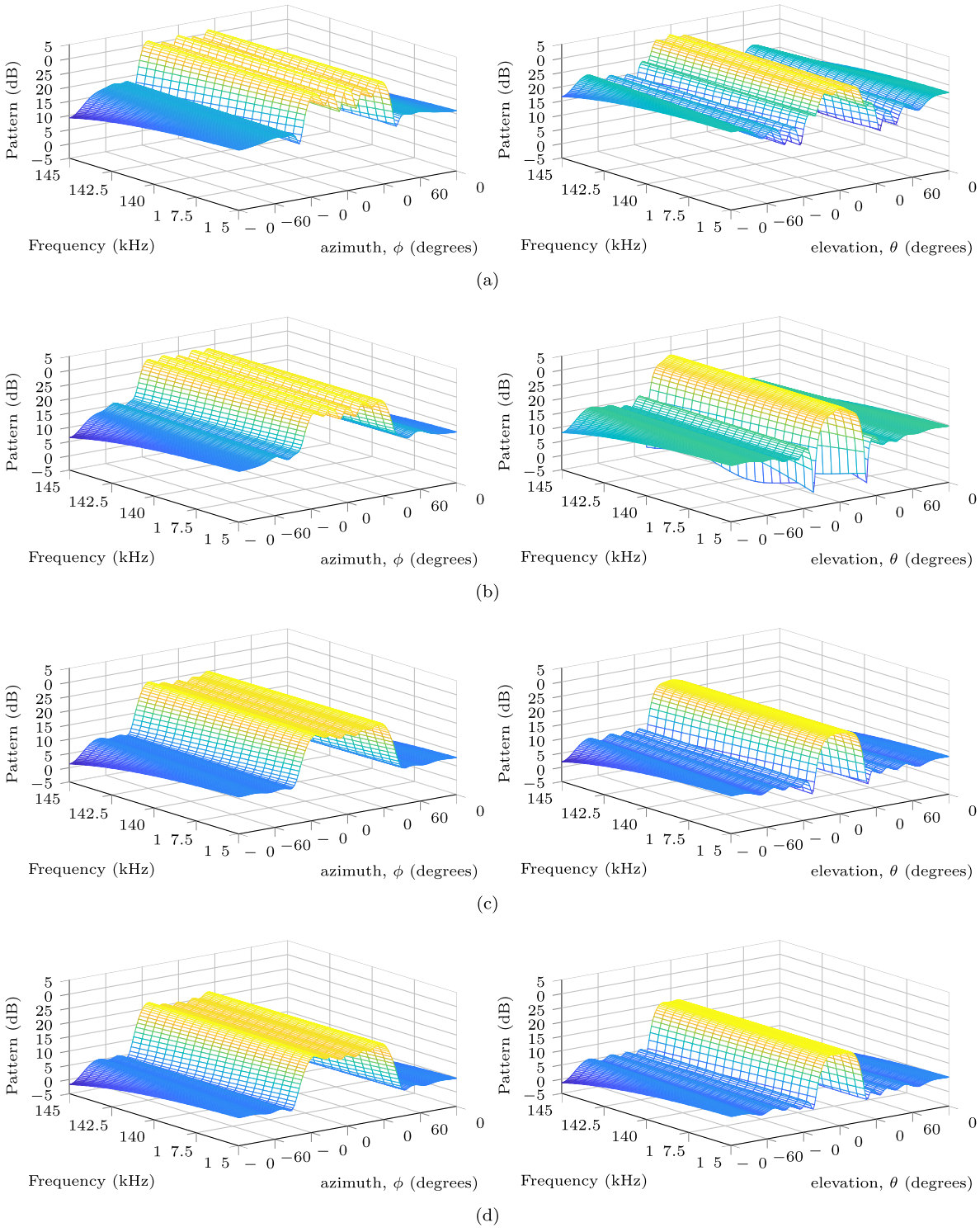

Fig. 8. For wideband transmit beamforming with 144 elements URA, beampattern on cutting-planes versus PAPR, (a) $\sigma = 1$, (b) $\sigma = 2$, (c) $\sigma = 8$ and (d) $\sigma = 36$.

the problem, we use the alternating direction method of multipliers (ADMM), which is capable of converging on a solution for the problems with convex objective function and nonconvex constraints. We combine the phase retrieval method PhareADMM [18] and the alternating projection method [11] through an ADMM formulation. For the beam shape and PAPR constraints, we make use of distinct penalty parameters in the augmented Lagrangian function. Thus, we can control the constraint violation of the beam shape and PAPR separately. Owing to the generality of formulation, the suggested method PAPR-ADMM can be applied both narrowband and wideband beamforming. Furthermore, depending on the application, a fast implementation with FFT can also be utilized. The method is not given specifically for the unimodular sequence design; but the results reveal that we can obtain competitive unimodular sequences by the suggested method PAPR-ADMM. Most importantly, the numerical results indicate that indeed a trade-off between high power efficiency and a good approximation to

the desired beampattern can be achieved by tuning the PAPR constraint. Finally, a ready-to-use MATLAB code is provided at [31].

Declaration of competing interest

The authors declare that they have no known competing financial interests or personal relationships that could have appeared to influence the work reported in this paper.

Acknowledgments

We would like to thank Yang Jing, Prof. Junli Liang and Prof. Hing Cheung So for kindly providing us with the MATLAB code of ANSLM and the figure data for ADMM and LPNN. Moreover, we would like to thank the anonymous reviewers for their comments and suggestions.

Appendix A. On PAPR constraint

A.1. Example problem

Consider a problem of finding the nearest vector to a given vector $\mathbf{s} \in \mathbb{C}^N$ under PAPR constraint. This problem can be stated as

$$\begin{aligned} \underset{\mathbf{w}\in\mathbb{C}^N}{\text{minimize}} \quad & \|\mathbf{w}-\mathbf{s}\|_2 \\ \text{subject to} \quad & \text{PAPR}(\mathbf{w}) \leqslant \sigma, \\ & \|\mathbf{w}\|_2^2 = P, \end{aligned} \tag{A.1}$$

and can be solved efficiently with an alternating projection method given in [11].

Readers should notice that the optimal vector $\mathbf{w}^\star$ and $\mathbf{s}$ always have the same phase independently of σ; since PAPR$(\cdot)$ does not depend on the phase of its argument, see (1). As expected, the solution is unimodular

$$\mathbf{w}^\star = \sqrt{\frac{P}{N}} e^{j\angle \mathbf{s}} \tag{A.2}$$

for the lower bound of PAPR, i.e., $\sigma = 1$. When $\sigma = N$, i.e., when PAPR constraint is inactive, the solution becomes

$$\mathbf{w}^\star = \frac{\sqrt{P}}{\|\mathbf{s}\|_2}\mathbf{s}. \tag{A.3}$$

Indeed, (A.3) is valid for PAPR$(\mathbf{s}) \leqslant \sigma \leqslant N$.

A.2. Example problem extension: variable total power

Consider the extension of (A.1), where P is added as an optimization variable as follows:

$$\begin{aligned} \underset{\mathbf{w}\in\mathbb{C}^N;\, P\in\mathbb{R}}{\text{minimize}} \quad & \|\mathbf{w}-\mathbf{s}\|_2^2 \\ \text{subject to} \quad & \text{PAPR}(\mathbf{w}) \leqslant \sigma, \\ & \|\mathbf{w}\|_2^2 = P. \end{aligned} \tag{A.4}$$

We can examine the effect of $\|\mathbf{w}\|_2^2 = P$ constraint on the objective function value of (A.1) by solving (A.4) for boundary PAPR values.

For the lower bound of PAPR, i.e., $\sigma = 1$, the solution $\mathbf{w}^\star$ can be expressed as a function of P, $\mathbf{w}^\star = \sqrt{P/N}e^{j\angle \mathbf{s}}$, as given in (A.2). According to this solution, the objective function can be expressed as

$$\begin{aligned} \|\mathbf{w}-\mathbf{s}\|_2^2 &= \|\mathbf{w}\|_2^2 - \mathbf{w}^{\mathrm{H}}\mathbf{s} - \mathbf{s}^{\mathrm{H}}\mathbf{w} + \|\mathbf{s}\|_2^2 \\ &= P - 2\sqrt{\frac{P}{N}}\sum_{n=1}^{N}|s_n| + \|\mathbf{s}\|_2^2, \end{aligned} \tag{A.5}$$

By differentiating (A.5) with respect to P and equating the result to zero, we find the minimizer of (A.5) as

$$P = \frac{1}{N}\left(\sum_{n=1}^{N}|s_n|\right)^2. \tag{A.6}$$

For the upper bound of PAPR, i.e., $\sigma = N$, the solution is $\mathbf{w}^\star = \sqrt{P}\,\mathbf{s}/\|\mathbf{s}\|_2$, as given in (A.3). Using this solution, we can express the objective function

$$\|\mathbf{w}-\mathbf{s}\|_2^2 = P - 2\sqrt{P}\|\mathbf{s}\|_2 + \|\mathbf{s}\|_2^2, \tag{A.7}$$

and the minimizer of (A.7) is

$$P = \|\mathbf{s}\|_2^2, \tag{A.8}$$

which is actually valid for PAPR$(\mathbf{s}) \leqslant \sigma \leqslant N$.

For the other values of PAPR, i.e., $1 < \sigma <$ PAPR$(\mathbf{s})$, there is no closed-form expression for $\mathbf{w}^\star$. Hence, there is no closed-form expression for P either; but the interval for P can be given as

$$\frac{1}{N}\left(\sum_{n=1}^{N}|s_n|\right)^2 < P < \|\mathbf{s}\|_2^2.$$

Furthermore, assuming that P_1 and P_2 are the minimizers for σ_1 and σ_2, respectively, if $\sigma_1 > \sigma_2$ then $P_1 > P_2$. It is obvious that (A.6) and (A.8) are equal only when PAPR$(\mathbf{s}) = 1$. Moreover, the objective function of (A.4) is zero only for $\sigma \geqslant$ PAPR$(\mathbf{s})$.

Lemma 1. *The achievable objective function value of (A.1) is zero if and only if $\sigma \geqslant$ PAPR$(\mathbf{s})$ and $P = \|\mathbf{s}\|_2^2$.*

Proof. Let $\mathbf{w}^\star$ be the solution of (A.1), then it is obvious that $\|\mathbf{w}^\star - \mathbf{s}\|_2 \geqslant 0$ and equality holds, i.e., the achievable objective function value of (A.1) is zero, only when $\mathbf{w}^\star = \mathbf{s}$. Two vectors $\mathbf{w}^\star$ and $\mathbf{s}$ are linearly dependent if and only if PAPR$(\mathbf{s}) \leqslant \sigma \leqslant N$, as given in (A.3). For (A.3), $\mathbf{w}^\star = \mathbf{s}$ if and only if $P = \|\mathbf{s}\|_2^2$. The proof is completed.

Appendix B. Equivalence of problems for updating auxiliary variables

To show the equivalence of (7) and (8), we proceed as follows:

$$\begin{aligned} &\sum_{n=1}^{N}\Re\left\{\lambda_n^{(k)}\right\}\Re\left\{w_n^{(k)}-v_n\right\} \\ &+\frac{\rho_N}{2}\sum_{n=1}^{N}\left(\Re\left\{w_n^{(k)}-v_n\right\}\right)^2 = -\frac{1}{2\rho_N}\sum_{n=1}^{N}\left(\Re\left\{\lambda_n^{(k)}\right\}\right)^2 \\ &\quad+\frac{\rho_N}{2}\sum_{n=1}^{N}\left(\Re\left\{w_n^{(k)}-v_n\right\}+\frac{1}{\rho_N}\Re\left\{\lambda_n^{(k)}\right\}\right)^2 \\ &\quad\quad= -\frac{1}{2\rho_N}\sum_{n=1}^{N}\left(\Re\left\{\lambda_n^{(k)}\right\}\right)^2 \\ &\quad+\frac{\rho_N}{2}\sum_{n=1}^{N}\left(\Re\left\{w_n^{(k)}-v_n+\tau_n^{(k)}\right\}\right)^2, \end{aligned} \tag{B.1}$$

where the first term is fixed since $\boldsymbol{\lambda}^{(k)}$ (and $\boldsymbol{\tau}^{(k)}$) is given for (7) in Step-1, and does not affect the arguments minimizing (7). After using this approach, namely, completing square and ignoring the constant terms, for the imaginary counterpart in (7), we can combine the expressions including real and imaginary parts for the

equivalent problem and get the last term of the objective function in (8) as

$$\begin{aligned}
&\frac{\rho_N}{2}\sum_{n=1}^{N}\left(\Re\left\{w_n^{(k)}-v_n+\tau_n^{(k)}\right\}\right)^2\\
&\quad+\frac{\rho_N}{2}\sum_{n=1}^{N}\left(\Im\left\{w_n^{(k)}-v_n+\tau_n^{(k)}\right\}\right)^2\\
&\quad=\frac{\rho_N}{2}\left(\mathbf{w}^{(k)}+\boldsymbol{\tau}^{(k)}-\mathbf{v}\right)^{\mathrm{H}}\left(\mathbf{w}^{(k)}+\boldsymbol{\tau}^{(k)}-\mathbf{v}\right)\\
&\quad=\frac{\rho_N}{2}\left\|\mathbf{w}^{(k)}+\boldsymbol{\tau}^{(k)}-\mathbf{v}\right\|_2^2. \qquad \text{(B.2)}
\end{aligned}$$

By applying the same procedure on the remaining terms corresponding to $\mathbf{y}^{(k)}$ (and $\mathbf{z}^{(k)}$), the equivalence of (7) and (8) can be shown. It should be noted that $\frac{\rho_L}{2}\sum_{\ell=1}^{L}\left|\mathbf{a}_\ell^{\mathrm{H}}\mathbf{w}^{(k)}+z_\ell^{(k)}-\alpha_\ell e^{j\beta_\ell}\right|^2$ in (8) can also be expressed in the form of (B.2) as

$$\frac{\rho_L}{2}\left\|\mathbf{A}^{\mathrm{H}}\mathbf{w}^{(k)}+\mathbf{z}^{(k)}-\boldsymbol{\alpha}\odot e^{j\boldsymbol{\beta}}\right\|_2^2.$$

Appendix C. Average power computation

Let the power function $\mathcal{P}$ corresponding to the sensor weights, $\mathbf{w}\in\mathbb{C}^N$, and the directions of transmitted (or received) signal, (ϕ,θ), be

$$\mathcal{P}_{\mathbf{w}}(\phi,\theta)=\left|\mathbf{a}(\phi,\theta)^{\mathrm{H}}\mathbf{w}\right|^2, \qquad \text{(C.1)}$$

where $\mathbf{a}(\phi,\theta)$ is the counterpart of $\mathbf{a}_\ell$ for continuous variables (ϕ,θ). Let $\mathcal{M}=\Phi_m\times\Theta_m=\{(\phi,\theta)|\phi\in\Phi_m,\theta\in\Theta_m\}$ and $\mathcal{S}=\Phi_s\times\Theta_s=\{(\phi,\theta)|\phi\in\Phi_s,\theta\in\Theta_s\}$ be the set of directions for mainlobe and sidelobe, respectively. Then, the mainlobe average power is defined as

$$P_{\text{avg}}^{\text{m}}\triangleq\frac{1}{|\mathcal{M}|}\iint\limits_{(\phi,\theta)\in\mathcal{M}}\mathcal{P}_{\mathbf{w}}(\phi,\theta)\,\mathrm{d}\phi\,\mathrm{d}\theta. \qquad \text{(C.2)}$$

The RHS of (C.2) can be expressed as $P_{\text{avg}}^{\text{m}}=\mathbf{w}^{\mathrm{H}}\mathbf{R}_{\mathcal{M}}\mathbf{w}$, where the $N\times N$ matrix $\mathbf{R}_{\mathcal{M}}$ is defined as

$$\mathbf{R}_{\mathcal{M}}\triangleq\frac{1}{|\mathcal{M}|}\iint\limits_{(\phi,\theta)\in\mathcal{M}}\mathbf{a}(\phi,\theta)\mathbf{a}(\phi,\theta)^{\mathrm{H}}\,\mathrm{d}\phi\,\mathrm{d}\theta \qquad \text{(C.3)}$$

and its (r,c) entry is

$$\mathbf{R}_{\mathcal{M}}[r,c]=\frac{1}{|\mathcal{M}|}\iint\limits_{(\phi,\theta)\in\mathcal{M}}e^{j\mathbf{k}(\phi,\theta)^{\mathrm{T}}(\mathbf{p}_r-\mathbf{p}_c)}\,\mathrm{d}\phi\,\mathrm{d}\theta \qquad \text{(C.4)}$$

for $r,c=1,\ldots,N$. Similarly, the sidelobe average power $P_{\text{avg}}^{\text{s}}$ can be defined by replacing $\mathcal{M}$ in (C.2) with $\mathcal{S}$. Then, the ratio of the average power in mainlobe and sidelobe is defined as $P_{\text{avg}}^{\text{m/s}}\triangleq P_{\text{avg}}^{\text{m}}/P_{\text{avg}}^{\text{s}}$.

References

[1] M.I. Skolnik, Radar Handbook, 3rd edition, McGraw-Hill, 2008.

[2] A. Mutapcic, S.-J. Kim, S. Boyd, Beamforming with uncertain weights, IEEE Signal Process. Lett. 14 (5) (2007) 348–351, https://doi.org/10.1109/LSP.2006.888102.

[3] H. Lebret, S. Boyd, Antenna array pattern synthesis via convex optimization, IEEE Trans. Signal Process. 45 (3) (1997) 526–532, https://doi.org/10.1109/78.558465.

[4] H. He, J. Li, P. Stoica, Waveform Design for Active Sensing Systems: A Computational Approach, Cambridge University Press, Cambridge, 2012.

[5] H. He, P. Stoica, J. Li, Wideband MIMO systems: signal design for transmit beampattern synthesis, IEEE Trans. Signal Process. 59 (2) (2011) 618–628, https://doi.org/10.1109/TSP.2010.2091410.

[6] M. Soltanalian, B. Tang, J. Li, P. Stoica, Joint design of the receive filter and transmit sequence for active sensing, IEEE Signal Process. Lett. 20 (5) (2013) 423–426, https://doi.org/10.1109/LSP.2013.2250279.

[7] Y. Tang, W. Sheng, Y.D. Zhang, M.G. Amin, Wideband multiple-input multiple-output radar waveform design with low peak-to-average ratio constraint, IET Radar Sonar Navig. 10 (2) (2016) 325–332, https://doi.org/10.1049/iet-rsn.2015.0189.

[8] H. Esmaeili-Najafabadi, M. Ataei, M.F. Sabahi, Designing sequence with minimum PSL using Chebyshev distance and its application for chaotic MIMO radar waveform design, IEEE Trans. Signal Process. 65 (3) (2017) 690–704, https://doi.org/10.1109/TSP.2016.2621728.

[9] Z. Cheng, Z. He, B. Liao, M. Fang, MIMO radar waveform design with PAPR and similarity constraints, IEEE Trans. Signal Process. 66 (4) (2018) 968–981, https://doi.org/10.1109/TSP.2017.2780052.

[10] M. Soltanalian, M.M. Naghsh, P. Stoica, A fast algorithm for designing complementary sets of sequences, Signal Process. 93 (7) (2013) 2096–2102, https://doi.org/10.1016/j.sigpro.2013.02.008.

[11] J. Tropp, I. Dhillon, R. Heath, T. Strohmer, Designing structured tight frames via an alternating projection method, IEEE Trans. Inf. Theory 51 (1) (2005) 188–209, https://doi.org/10.1109/TIT.2004.839492.

[12] L. Tang, Y. Zhu, Q. Fu, Designing PAR-constrained periodic/aperiodic sequence via the gradient-based method, Signal Process. 147 (2018) 11–22, https://doi.org/10.1016/j.sigpro.2018.01.006.

[13] H. Griffiths, L. Cohen, S. Watts, E. Mokole, C. Baker, M. Wicks, S. Blunt, Radar spectrum engineering and management: technical and regulatory issues, Proc. IEEE 103 (1) (2015) 85–102, https://doi.org/10.1109/JPROC.2014.2365517.

[14] J. Song, P. Babu, D.P. Palomar, Optimization methods for designing sequences with low autocorrelation sidelobes, IEEE Trans. Signal Process. 63 (15) (2015) 3998–4009, https://doi.org/10.1109/TSP.2015.2425808.

[15] J. Liang, H.C. So, C.S. Leung, J. Li, A. Farina, Waveform design with unit modulus and spectral shape constraints via Lagrange programming neural network, IEEE J. Sel. Top. Signal Process. 9 (8) (2015) 1377–1386, https://doi.org/10.1109/JSTSP.2015.2464178.

[16] J. Song, P. Babu, D.P. Palomar, Sequence design to minimize the weighted integrated and peak sidelobe levels, IEEE Trans. Signal Process. 64 (8) (2016) 2051–2064, https://doi.org/10.1109/TSP.2015.2510982.

[17] J. Liang, H.C. So, J. Li, A. Farina, Unimodular sequence design based on alternating direction method of multipliers, IEEE Trans. Signal Process. 64 (20) (2016) 5367–5381, https://doi.org/10.1109/TSP.2016.2597123.

[18] J. Liang, P. Stoica, Y. Jing, J. Li, Phase retrieval via the alternating direction method of multipliers, IEEE Signal Process. Lett. 25 (1) (2018) 5–9, https://doi.org/10.1109/LSP.2017.2767826, arXiv:1808.05802.

[19] J. Liang, H. So, J. Li, A. Farina, D. Zhou, On optimizations with magnitude constraints on frequency or angular responses, Signal Process. 145 (2018) 214–224, https://doi.org/10.1016/j.sigpro.2017.12.009.

[20] W. Rowe, P. Stoica, J. Li, Spectrally constrained waveform design, IEEE Signal Process. Mag. 31 (3) (2014) 157–162, https://doi.org/10.1109/MSP.2014.2301792.

[21] Y. Jing, J. Liang, D. Zhou, H.C. So, Spectrally constrained unimodular sequence design without spectral level mask, IEEE Signal Process. Lett. 25 (7) (2018) 1004–1008, https://doi.org/10.1109/LSP.2018.2836219.

[22] S. Boyd, N. Parikh, E. Chu, B. Peleato, J. Eckstein, Distributed optimization and statistical learning via the alternating direction method of multipliers, Found. Trends Mach. Learn. 3 (1) (2010) 1–122, https://doi.org/10.1561/2200000016, arXiv:1408.2927.

[23] R. Nishihara, L. Lessard, B. Recht, A. Packard, M. Jordan, A general analysis of the convergence of ADMM, in: F. Bach, D. Blei (Eds.), Proceedings of the 32nd International Conference on Machine Learning, in: Proceedings of Machine Learning Research, vol. 37, PMLR, Lille, France, 2015, pp. 343–352.

[24] M.J.D. Powell, A method for nonlinear constraints in minimization problems, in: R. Fletcher (Ed.), Optimization, Academic Press, New York, NY, 1969, pp. 283–298.

[25] D.P. Bertsekas, Multiplier methods: a survey, in: IFAC Proceedings, vols. 8 (1), 1975, pp. 351–363, https://doi.org/10.1016/S1474-6670(17)67759-0.

[26] R. Fletcher, Practical Methods of Optimization, 2nd edition, John Wiley & Sons, Ltd, Chichester, West Sussex England, 1987.

[27] M.R. Hestenes, Multiplier and gradient methods, J. Optim. Theory Appl. 4 (5) (1969) 303–320, https://doi.org/10.1007/BF00927673.

[28] D.P. Bertsekas, On penalty and multiplier methods for constrained minimization, in: O.L. Mangasarian, R.R. Meyer, S.M. Robinson (Eds.), Nonlinear Programming 2, Elsevier, 1975, pp. 165–191.

[29] M.S. Bazaraa, H.D. Sherali, C.M. Shetty, Nonlinear Programming, John Wiley & Sons, Inc., Hoboken, NJ, USA, 2006.

[30] C. Candan, Properly handling complex differentiation in optimization and approximation problems, IEEE Signal Process. Mag. 36 (2) (2019) 117–124, https://doi.org/10.1109/MSP.2018.2876761.

[31] Ö. Çayır, Ç. Candan, Transmit beamformer design with a PAPR constraint to trade-off between beampattern shape and power efficiency (MATLAB code), https://doi.org/10.24433/CO.7886035.v1, 2019.

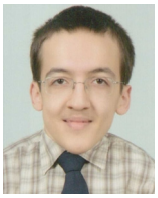

Ömer Çayır received the B.S. degree (with rank 1) from Hacettepe University, Ankara, Turkey, in 2011, and the M.S. degree from Middle East Technical University, Ankara, in 2014, both in electrical and electronic engineering, and is currently working toward the Ph.D. degree with the Department of Electrical and Electronics Engineering, Middle East Technical University, Ankara.

He is currently a Research Assistant with the Department of Electrical and Electronics Engineering, Middle East Technical University. His research interests include statistical signal processing and its applications in waveform optimization, stochastic control, radar resource management, and software defined radio.

Çağatay Candan received the B.S. degree from Middle East Technical University, Ankara, Turkey, in 1996, the M.S. degree from Bilkent University, Ankara, in 1998, and the Ph.D. degrees from Georgia Institute of Technology, Atlanta, GA, USA, in 2004, respectively, all in electrical engineering.

He is currently a Professor with the Department of Electrical and Electronics Engineering, Middle East Technical University. His research interests include statistical signal processing and its applications in array signal processing, radar signal processing and communications.